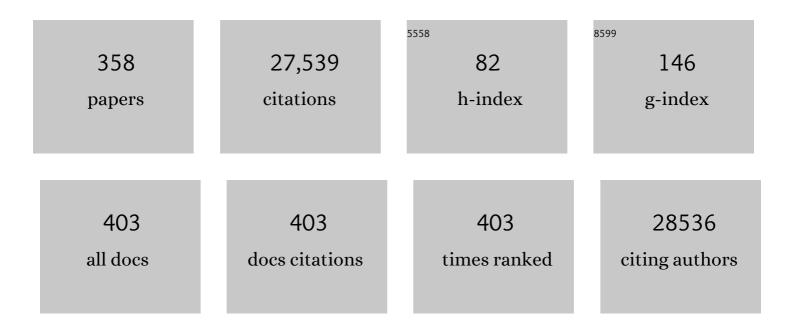
List of Publications by Year in descending order

Source: https://exaly.com/author-pdf/6659204/publications.pdf Version: 2024-02-01



#	Article	IF	CITATIONS
1	Electron crystallography of chiral and non-chiral small molecules. Ultramicroscopy, 2022, 232, 113417.	0.8	2
2	Cryo-EM analysis of Ebola virus nucleocapsid-like assembly. STAR Protocols, 2022, 3, 101030.	0.5	0
3	Capturing the swelling of solid-electrolyte interphase in lithium metal batteries. Science, 2022, 375, 66-70.	6.0	183
4	Cryo-EM, Protein Engineering, and Simulation Enable the Development of Peptide Therapeutics against Acute Myeloid Leukemia. ACS Central Science, 2022, 8, 214-222.	5.3	7
5	Cryo-ET of <i>Toxoplasma</i> parasites gives subnanometer insight into tubulin-based structures. Proceedings of the National Academy of Sciences of the United States of America, 2022, 119, .	3.3	26
6	Methods and Applications of Campenot Trichamber Neuronal Cultures for the Study of Neuroinvasive Viruses. Methods in Molecular Biology, 2022, 2431, 181-206.	0.4	6
7	Planar 2D wireframe DNA origami. Science Advances, 2022, 8, .	4.7	10
8	Chikungunya virus assembly and budding visualized in situ using cryogenic electron tomography. Nature Microbiology, 2022, 7, 1270-1279.	5.9	21
9	Cathode-Electrolyte Interphase in Lithium Batteries Revealed by Cryogenic Electron Microscopy. Matter, 2021, 4, 302-312.	5.0	127
10	Three-Dimensional Analysis of Particle Distribution on Filter Layers inside N95 Respirators by Deep Learning. Nano Letters, 2021, 21, 651-657.	4.5	41
11	The N-terminus of varicella-zoster virus glycoprotein B has a functional role in fusion. PLoS Pathogens, 2021, 17, e1008961.	2.1	12
12	A Single Immunization with Spike-Functionalized Ferritin Vaccines Elicits Neutralizing Antibody Responses against SARS-CoV-2 in Mice. ACS Central Science, 2021, 7, 183-199.	5.3	134
13	Cryo-Electron Microscopy (CEM) Structures of Viruses. , 2021, , 233-241.		1
14	Evolution of standardization and dissemination of cryo-EM structures and data jointly by the community, PDB, and EMDB. Journal of Biological Chemistry, 2021, 296, 100560.	1.6	18
15	Cryo-EM model validation recommendations based on outcomes of the 2019 EMDataResource challenge. Nature Methods, 2021, 18, 156-164.	9.0	73
16	Structural analyses of an RNA stability element interacting with poly(A). Proceedings of the National Academy of Sciences of the United States of America, 2021, 118, .	3.3	13
17	Preface. Progress in Biophysics and Molecular Biology, 2021, 160, 1.	1.4	0
18	Structural and functional dissection of reovirus capsid folding and assembly by the prefoldin-TRiC/CCT chaperone network. Proceedings of the National Academy of Sciences of the United States of America, 2021, 118, .	3.3	30

Waн Chiu

#	Article	IF	CITATIONS
19	RNA nanotechnology to build a dodecahedral genome of single-stranded RNA virus. RNA Biology, 2021, 18, 2390-2400.	1.5	8
20	REMBI: Recommended Metadata for Biological Images—enabling reuse of microscopy data in biology. Nature Methods, 2021, 18, 1418-1422.	9.0	63
21	Regulation of reversible conformational change, size switching, and immunomodulation of RNA nanocubes. Rna, 2021, 27, 971-980.	1.6	2
22	Explore the complexity of proteins with an expanded CryoET data processing pipeline. Microscopy and Microanalysis, 2021, 27, 2816-2817.	0.2	0
23	CryoEM Map-Model Scores: From Average Density to Q-scores. Microscopy and Microanalysis, 2021, 27, 1382-1384.	0.2	1
24	Cryogenic Electron Microscopy for Energy Materials. Accounts of Chemical Research, 2021, 54, 3505-3517.	7.6	19
25	Cryo-electron tomography provides topological insights into mutant huntingtin exon 1 and polyQ aggregates. Communications Biology, 2021, 4, 849.	2.0	19
26	Resolve cathode electrolyte interphase in lithium batteries with cryo-EM. Microscopy and Microanalysis, 2021, 27, 2188-2190.	0.2	0
27	High Resolution Data Collection at S2C2, a National CryoEM Center. Microscopy and Microanalysis, 2021, 27, 1152-1154.	0.2	0
28	Validation, analysis and annotation of cryo-EM structures. Acta Crystallographica Section D: Structural Biology, 2021, 77, 1142-1152.	1.1	14
29	CryoEM reveals the stochastic nature of individual ATP binding events in a group II chaperonin. Nature Communications, 2021, 12, 4754.	5.8	9
30	Cryo-EM and antisense targeting of the 28-kDa frameshift stimulation element from the SARS-CoV-2 RNA genome. Nature Structural and Molecular Biology, 2021, 28, 747-754.	3.6	91
31	Cryo-EM structures of full-length Tetrahymena ribozyme at 3.1ÂÃ resolution. Nature, 2021, 596, 603-607.	13.7	59
32	Rapid prototyping of arbitrary 2D and 3D wireframe DNA origami. Nucleic Acids Research, 2021, 49, 10265-10274.	6.5	51
33	Target highlights in <scp>CASP14</scp> : Analysis of models by structure providers. Proteins: Structure, Function and Bioinformatics, 2021, 89, 1647-1672.	1.5	27
34	Altered Cardiac Energetics and Mitochondrial Dysfunction in Hypertrophic Cardiomyopathy. Circulation, 2021, 144, 1714-1731.	1.6	90
35	Mapping the catalytic conformations of an assembly-line polyketide synthase module. Science, 2021, 374, 729-734.	6.0	41
36	The N-terminus of varicella-zoster virus glycoprotein B has a functional role in fusion. , 2021, 17, e1008961.		0

#	Article	IF	CITATIONS
37	The N-terminus of varicella-zoster virus glycoprotein B has a functional role in fusion. , 2021, 17, e1008961.		0
38	The N-terminus of varicella-zoster virus glycoprotein B has a functional role in fusion. , 2021, 17, e1008961.		0
39	The N-terminus of varicella-zoster virus glycoprotein B has a functional role in fusion. , 2021, 17, e1008961.		Ο
40	Cryo-EM and MD infer water-mediated proton transport and autoinhibition mechanisms of V _o complex. Science Advances, 2020, 6, .	4.7	51
41	Full-length three-dimensional structure of the influenza A virus M1 protein and its organization into a matrix layer. PLoS Biology, 2020, 18, e3000827.	2.6	20
42	Cryo-EM Structures of Atomic Surfaces and Host-Guest Chemistry in Metal-Organic Frameworks. Matter, 2020, 2, 1064.	5.0	2
43	Cryogenic Correlative Singleâ€Particle Photoluminescence Spectroscopy and Electron Tomography for Investigation of Nanomaterials. Angewandte Chemie, 2020, 132, 15772-15778.	1.6	1
44	Opportunities for Cryogenic Electron Microscopy in Materials Science and Nanoscience. ACS Nano, 2020, 14, 9263-9276.	7.3	55
45	Multi-scale 3D Cryo-Correlative Microscopy for Vitrified Cells. Structure, 2020, 28, 1231-1237.e3.	1.6	60
46	3D RNA nanocage for encapsulation and shielding of hydrophobic biomolecules to improve the in vivo biodistribution. Nano Research, 2020, 13, 3241-3247.	5.8	4
47	Unique cellular protrusions mediate breast cancer cell migration by tethering to osteogenic cells. Npj Breast Cancer, 2020, 6, 42.	2.3	14
48	Decontamination of SARS-CoV-2 and Other RNA Viruses from N95 Level Meltblown Polypropylene Fabric Using Heat under Different Humidities. ACS Nano, 2020, 14, 14017-14025.	7.3	69
49	A glycoprotein B-neutralizing antibody structure at 2.8 à uncovers a critical domain for herpesvirus fusion initiation. Nature Communications, 2020, 11, 4141.	5.8	23
50	A 3.4-Ã cryo-electron microscopy structure of the human coronavirus spike trimer computationally derived from vitrified NL63 virus particles. QRB Discovery, 2020, 1, e11.	0.6	10
51	Resolving individualÂatoms of protein complex by cryo-electron microscopy. Cell Research, 2020, 30, 1136-1139.	5.7	69
52	Sub-Ãngström-resolution MicroED Using a Direct Detection Camera. Microscopy and Microanalysis, 2020, 26, 1524-1526.	0.2	0
53	Cryogenic single-molecule fluorescence annotations for electron tomography reveal in situ organization of key proteins in <i>Caulobacter</i> . Proceedings of the National Academy of Sciences of the United States of America, 2020, 117, 13937-13944.	3.3	73
54	Cryo-EM structures of NPC1L1 reveal mechanisms of cholesterol transport and ezetimibe inhibition. Science Advances, 2020, 6, eabb1989.	4.7	49

#	Article	IF	CITATIONS
55	Cryo-EM Structures of Human Drosha and DGCR8 in Complex with Primary MicroRNA. Molecular Cell, 2020, 78, 411-422.e4.	4.5	75
56	Accelerated cryo-EM-guided determination of three-dimensional RNA-only structures. Nature Methods, 2020, 17, 699-707.	9.0	119
57	Structure of the G protein chaperone and guanine nucleotide exchange factor Ric-8A bound to Gαi1. Nature Communications, 2020, 11, 1077.	5.8	18
58	Arrangement of the Polymerase Complexes inside a Nine-Segmented dsRNA Virus. Structure, 2020, 28, 604-612.e3.	1.6	10
59	Ultra-thermostable RNA nanoparticles for solubilizing and high-yield loading of paclitaxel for breast cancer therapy. Nature Communications, 2020, 11, 972.	5.8	86
60	Measurement of atom resolvability in cryo-EM maps with Q-scores. Nature Methods, 2020, 17, 328-334.	9.0	230
61	TrkA undergoes a tetramer-to-dimer conversion to open TrkH which enables changes in membrane potential. Nature Communications, 2020, 11, 547.	5.8	20
62	Cryogenic Correlative Singleâ€Particle Photoluminescence Spectroscopy and Electron Tomography for Investigation of Nanomaterials. Angewandte Chemie - International Edition, 2020, 59, 15642-15648.	7.2	8
63	Inhibition mechanisms of AcrF9, AcrF8, and AcrF6 against type I-F CRISPR–Cas complex revealed by cryo-EM. Proceedings of the National Academy of Sciences of the United States of America, 2020, 117, 7176-7182.	3.3	35
64	Evolving data standards for cryo-EM structures. Structural Dynamics, 2020, 7, 014701.	0.9	26
65	Title is missing!. , 2020, 18, e3000827.		0
66	Title is missing!. , 2020, 18, e3000827.		0
67	Title is missing!. , 2020, 18, e3000827.		0
68	Title is missing!. , 2020, 18, e3000827.		0
69	Redox Engineering of Cytochrome c using DNA Nanostructure-Based Charged Encapsulation and Spatial Control. ACS Applied Materials & Interfaces, 2019, 11, 13874-13880.	4.0	27
70	Stanford-SLAC Cryo-EM Center (S ² C ²). Microscopy and Microanalysis, 2019, 25, 2658-2659.	0.2	1
71	Cryoâ€electron microscopy targets in CASP13: Overview and evaluation of results. Proteins: Structure, Function and Bioinformatics, 2019, 87, 1128-1140.	1.5	21
72	Cryo-EM Study of Chaperonin Mm-Cpn's Conformational Heterogeneity under Different ATP Conditions. Microscopy and Microanalysis, 2019, 25, 1006-1007.	0.2	1

#	Article	IF	CITATIONS
73	Unravelling Degradation Mechanisms and Atomic Structure of Organic-Inorganic Halide Perovskites by Cryo-EM. Joule, 2019, 3, 2854-2866.	11.7	99
74	Segmentation and Comparative Modeling in an 8.6-Ã Cryo-EM Map of the Singapore Grouper Iridovirus. Structure, 2019, 27, 1561-1569.e4.	1.6	10
75	Cryo-EM Structures of Atomic Surfaces and Host-Guest Chemistry in Metal-Organic Frameworks. Matter, 2019, 1, 428-438.	5.0	102
76	Cryo-EM structures of <i>Helicobacter pylori</i> vacuolating cytotoxin A oligomeric assemblies at near-atomic resolution. Proceedings of the National Academy of Sciences of the United States of America, 2019, 116, 6800-6805.	3.3	33
77	Coupling of ssRNA cleavage with DNase activity in type III-A CRISPR-Csm revealed by cryo-EM and biochemistry. Cell Research, 2019, 29, 305-312.	5.7	40
78	The Chaperonin TRiC/CCT Associates with Prefoldin through a Conserved Electrostatic Interface Essential for Cellular Proteostasis. Cell, 2019, 177, 751-765.e15.	13.5	98
79	Structural basis of amino acid surveillance by higher-order tRNA-mRNA interactions. Nature Structural and Molecular Biology, 2019, 26, 1094-1105.	3.6	52
80	Cryo-EM structure of a 40ÂkDa SAM-IV riboswitch RNA at 3.7 à resolution. Nature Communications, 2019, 10, 5511.	5.8	90
81	Photo-controlled release of paclitaxel and model drugs from RNA pyramids. Nano Research, 2019, 12, 41-48.	5.8	32
82	Structure of Calcarisporiella thermophila Hsp104 Disaggregase that Antagonizes Diverse Proteotoxic Misfolding Events. Structure, 2019, 27, 449-463.e7.	1.6	29
83	Structures of TRPV2 in distinct conformations provide insight into role of the pore turret. Nature Structural and Molecular Biology, 2019, 26, 40-49.	3.6	47
84	Automated Sequence Design of 3D Polyhedral Wireframe DNA Origami with Honeycomb Edges. ACS Nano, 2019, 13, 2083-2093.	7.3	77
85	Electron Cryo-microscopy Structure of Ebola Virus Nucleoprotein Reveals a Mechanism for Nucleocapsid-like Assembly. Cell, 2018, 172, 966-978.e12.	13.5	51
86	The 3.5-Ã CryoEM Structure of Nanodisc-Reconstituted Yeast Vacuolar ATPase Vo Proton Channel. Molecular Cell, 2018, 69, 993-1004.e3.	4.5	103
87	Structure of the 30ÂkDa HIV-1 RNA Dimerization Signal by a Hybrid Cryo-EM, NMR, and Molecular Dynamics Approach. Structure, 2018, 26, 490-498.e3.	1.6	52
88	Purification of AcrAB-TolC Multidrug Efflux Pump for Cryo-EM Analysis. Methods in Molecular Biology, 2018, 1700, 71-81.	0.4	0
89	Novel Insect-Specific Eilat Virus-Based Chimeric Vaccine Candidates Provide Durable, Mono- and Multivalent, Single-Dose Protection against Lethal Alphavirus Challenge. Journal of Virology, 2018, 92, .	1.5	44
90	Distribution of evaluation scores for the models submitted to the second cryo-EM model challenge. Data in Brief, 2018, 20, 1629-1638.	0.5	5

#	Article	IF	CITATIONS
91	Machining protein microcrystals for structure determination by electron diffraction. Proceedings of the United States of America, 2018, 115, 9569-9573.	3.3	69
92	GENFIRE: from Precisely Localizing Single Atoms in Materials to High Resolution 3D Imaging of Cellular Structures. Microscopy and Microanalysis, 2018, 24, 1446-1447.	0.2	0
93	Programming molecular topologies from single-stranded nucleic acids. Nature Communications, 2018, 9, 4579.	5.8	39
94	Assessment of structural features in Cryo-EM density maps using SSE and side chain Z-scores. Journal of Structural Biology, 2018, 204, 564-571.	1.3	23
95	Evaluation system and web infrastructure for the second cryo-EM model challenge. Journal of Structural Biology, 2018, 204, 96-108.	1.3	11
96	The first single particle analysis Map Challenge: A summary of the assessments. Journal of Structural Biology, 2018, 204, 291-300.	1.3	17
97	Neutralizing Antibodies Inhibit Chikungunya Virus Budding at the Plasma Membrane. Cell Host and Microbe, 2018, 24, 417-428.e5.	5.1	56
98	Visualizing Individual RuBisCO and Its Assembly into Carboxysomes in Marine Cyanobacteria by Cryo-Electron Tomography. Journal of Molecular Biology, 2018, 430, 4156-4167.	2.0	63
99	Flagellum couples cell shape to motility in <i>Trypanosoma brucei</i> . Proceedings of the National Academy of Sciences of the United States of America, 2018, 115, E5916-E5925.	3.3	29
100	Accurate model annotation of a near-atomic resolution cryo-EM map. Proceedings of the National Academy of Sciences of the United States of America, 2017, 114, 3103-3108.	3.3	111
101	Novel Mechanism of Gating in the TrkH-TrkA Complex. Biophysical Journal, 2017, 112, 21a-22a.	0.2	0
102	Visualizing Adsorption of Cyanophage P-SSP7 onto Marine Prochlorococcus. Scientific Reports, 2017, 7, 44176.	1.6	24
103	SuRVoS: Super-Region Volume Segmentation workbench. Journal of Structural Biology, 2017, 198, 43-53.	1.3	72
104	A chikungunya fever vaccine utilizing an insect-specific virus platform. Nature Medicine, 2017, 23, 192-199.	15.2	105
105	Programmable Supraâ€Assembly of a DNA Surface Adapter for Tunable Chiral Directional Selfâ€Assembly of Gold Nanorods. Angewandte Chemie - International Edition, 2017, 56, 14632-14636.	7.2	76
106	Programmable Supraâ€Assembly of a DNA Surface Adapter for Tunable Chiral Directional Selfâ€Assembly of Gold Nanorods. Angewandte Chemie, 2017, 129, 14824-14828.	1.6	20
107	Responses to <i>`Atomic resolution': a badly abused term in structural biology</i> . Acta Crystallographica Section D: Structural Biology, 2017, 73, 381-383.	1.1	7
108	Structural and Functional Impacts of ER Coactivator Sequential Recruitment. Molecular Cell, 2017, 67, 733-743.e4.	4.5	69

#	Article	IF	CITATIONS
109	Convolutional neural networks for automated annotation of cellular cryo-electron tomograms. Nature Methods, 2017, 14, 983-985.	9.0	298
110	GENFIRE: A generalized Fourier iterative reconstruction algorithm for high-resolution 3D imaging. Scientific Reports, 2017, 7, 10409.	1.6	71
111	Subunit conformational variation within individual GroEL oligomers resolved by Cryo-EM. Proceedings of the National Academy of Sciences of the United States of America, 2017, 114, 8259-8264.	3.3	86
112	Electron Cryomicroscopy of Viruses at Near-Atomic Resolutions. Annual Review of Virology, 2017, 4, 287-308.	3.0	25
113	Editorial overview: Cryo Electron Microscopy: Exciting advances in CryoEM Herald a new era in structural biology. Current Opinion in Structural Biology, 2017, 46, iv-viii.	2.6	17
114	Influence of DNA sequence on the structure of minicircles under torsional stress. Nucleic Acids Research, 2017, 45, 7633-7642.	6.5	32
115	Going Deeper in Cryo Electron Tomography with Neural Networks. Microscopy and Microanalysis, 2017, 23, 814-815.	0.2	0
116	An allosteric transport mechanism for the AcrAB-TolC multidrug efflux pump. ELife, 2017, 6, .	2.8	190
117	Controllable Selfâ€Assembly of RNA Tetrahedrons with Precise Shape and Size for Cancer Targeting. Advanced Materials, 2016, 28, 7501-7507.	11.1	70
118	Quantifying Variability of Manual Annotation in Cryo-Electron Tomograms. Microscopy and Microanalysis, 2016, 22, 487-496.	0.2	22
119	Designer nanoscale DNA assemblies programmed from the top down. Science, 2016, 352, 1534-1534.	6.0	500
120	Alignment algorithms and per-particle CTF correction for single particle cryo-electron tomography. Journal of Structural Biology, 2016, 194, 383-394.	1.3	42
121	TRiC subunits enhance BDNF axonal transport and rescue striatal atrophy in Huntington's disease. Proceedings of the National Academy of Sciences of the United States of America, 2016, 113, E5655-64.	3.3	74
122	Visualizing red blood cell sickling and the effects of inhibition of sphingosine kinase 1 using soft x-ray tomography. Journal of Cell Science, 2016, 129, 3511-7.	1.2	21
123	Fabrication of RNA 3D Nanoprisms for Loading and Protection of Small RNAs and Model Drugs. Advanced Materials, 2016, 28, 10079-10087.	11.1	54
124	Chaperonin TRiC/CCT Recognizes Fusion Oncoprotein AML1-ETO through Subunit-Specific Interactions. Biophysical Journal, 2016, 110, 2377-2385.	0.2	12
125	Structure of the AcrABZ-TolC Multidrug Efflux Pump in a Drug-Bound State. Biophysical Journal, 2016, 110, 10a.	0.2	0
126	Resolution and Probabilistic Models of Components in CryoEM Maps of Mature P22 Bacteriophage. Biophysical Journal, 2016, 110, 827-839.	0.2	43

#	Article	IF	CITATIONS
127	EMDataBank unified data resource for 3DEM. Nucleic Acids Research, 2016, 44, D396-D403.	6.5	230
128	Resolution and Probabilistic Structural Models of Subcomponents Derived from CryoEM Maps of Mature P22 Bacteriophage. Biophysical Journal, 2016, 110, 158a.	0.2	0
129	The Electron Microscopy eXchange (EMX) initiative. Journal of Structural Biology, 2016, 194, 156-163.	1.3	12
130	Computational Tools to Improve Visualization by Cryo-Electron Tomography. Biophysical Journal, 2016, 110, 159a.	0.2	2
131	Chaperonin TRiC/CCT Modulates the Folding and Activity of Leukemogenic Fusion Oncoprotein AML1-ETO. Journal of Biological Chemistry, 2016, 291, 4732-4741.	1.6	25
132	Control of the structural landscape and neuronal proteotoxicity of mutant Huntingtin by domains flanking the polyQ tract. ELife, 2016, 5, .	2.8	62
133	Contribution of the Type II Chaperonin, TRiC/CCT, to Oncogenesis. International Journal of Molecular Sciences, 2015, 16, 26706-26720.	1.8	65
134	Modeling Protein Structure in Macromolecular Assemblies at Near Atomic Resolutions. Microscopy and Microanalysis, 2015, 21, 541-542.	0.2	0
135	IP3R1 - Assessing Map Interpretability at Near Atomic Resolution. Microscopy and Microanalysis, 2015, 21, 543-544.	0.2	0
136	Zernike Phase Plate Configuration at Intermediate Lens Position on JEM2200FS. Microscopy and Microanalysis, 2015, 21, 2143-2144.	0.2	1
137	Optimization of JEM2200FS for Zernike Phase Contrast Cryo-EM. Microscopy and Microanalysis, 2015, 21, 1577-1578.	0.2	1
138	Electron cryotomography reveals ultrastructure alterations in platelets from patients with ovarian cancer. Proceedings of the National Academy of Sciences of the United States of America, 2015, 112, 14266-14271.	3.3	61
139	Structure of a Biologically Active Estrogen Receptor-Coactivator Complex on DNA. Molecular Cell, 2015, 57, 1047-1058.	4.5	137
140	Lemon-shaped halo archaeal virus His1 with uniform tail but variable capsid structure. Proceedings of the United States of America, 2015, 112, 2449-2454.	3.3	43
141	An Intrinsically Disordered Peptide from Ebola Virus VP35 Controls Viral RNA Synthesis by Modulating Nucleoprotein-RNA Interactions. Cell Reports, 2015, 11, 376-389.	2.9	136
142	Structural Mechanisms of Mutant Huntingtin Aggregation Suppression by the Synthetic Chaperonin-like CCT5 Complex Explained by Cryoelectron Tomography. Journal of Biological Chemistry, 2015, 290, 17451-17461.	1.6	35
143	Outcome of the First wwPDB Hybrid/Integrative Methods Task Force Workshop. Structure, 2015, 23, 1156-1167.	1.6	159
144	CTF Challenge: Result summary. Journal of Structural Biology, 2015, 190, 348-359.	1.3	34

#	Article	IF	CITATIONS
145	Gating machinery of InsP3R channels revealed by electron cryomicroscopy. Nature, 2015, 527, 336-341.	13.7	199
146	Structural diversity of supercoiled DNA. Nature Communications, 2015, 6, 8440.	5.8	122
147	Improved Peak Detection and Deconvolution of Native Electrospray Mass Spectra from Large Protein Complexes. Journal of the American Society for Mass Spectrometry, 2015, 26, 2141-2151.	1.2	49
148	The pseudo-atomic structure of an RND-type tripartite multidrug efflux pump. Biological Chemistry, 2015, 396, 1073-1082.	1.2	10
149	A Newly Isolated Reovirus Has the Simplest Genomic and Structural Organization of Any Reovirus. Journal of Virology, 2015, 89, 676-687.	1.5	50
150	Modulation of STAT3 Folding and Function by TRiC/CCT Chaperonin. PLoS Biology, 2014, 12, e1001844.	2.6	84
151	A Structural Model of the Genome Packaging Process in a Membrane-Containing Double Stranded DNA Virus. PLoS Biology, 2014, 12, e1002024.	2.6	41
152	An atomic model of brome mosaic virus using direct electron detection and real-space optimization. Nature Communications, 2014, 5, 4808.	5.8	105
153	A 3D cellular context for the macromolecular world. Nature Structural and Molecular Biology, 2014, 21, 841-845.	3.6	47
154	Protruding knob-like proteins violate local symmetries in an icosahedral marine virus. Nature Communications, 2014, 5, 4278.	5.8	21
155	Zernike phase-contrast electron cryotomography applied to marine cyanobacteria infected with cyanophages. Nature Protocols, 2014, 9, 2630-2642.	5.5	24
156	Preparation of Primary Neurons for Visualizing Neurites in a Frozen-hydrated State Using Cryo-Electron Tomography. Journal of Visualized Experiments, 2014, , e50783.	0.2	10
157	Multiple Functional Roles of the Accessory I-Domain of Bacteriophage P22 Coat Protein Revealed by NMR Structure and CryoEM Modeling. Structure, 2014, 22, 830-841.	1.6	40
158	Structure of the AcrAB–TolC multidrug efflux pump. Nature, 2014, 509, 512-515.	13.7	519
159	Capsid expansion mechanism of bacteriophage T7 revealed by multistate atomic models derived from cryo-EM reconstructions. Proceedings of the National Academy of Sciences of the United States of America, 2014, 111, E4606-14.	3.3	87
160	Crystal structure of a nematode-infecting virus. Proceedings of the National Academy of Sciences of the United States of America, 2014, 111, 12781-12786.	3.3	28
161	Multifunctional RNA Nanoparticles. Nano Letters, 2014, 14, 5662-5671.	4.5	181
162	Reprogramming an ATP-Driven Biological Machine into a Light-Gated Protein Nanocage. Biophysical Journal, 2014, 106, 439a.	0.2	0

Waн Chiu

#	Article	IF	CITATIONS
163	Cryo-EM Studies of RyR1 Channel in Detergent-Free Aqueous Environment. Biophysical Journal, 2014, 106, 109a.	0.2	0
164	Editorial overview: Virus structure and function. Current Opinion in Virology, 2014, 5, viii-ix.	2.6	0
165	Chaperoninâ€containing TCPâ€1 complex directly binds to the cytoplasmic domain of the LOXâ€1 receptor. FEBS Letters, 2014, 588, 2133-2140.	1.3	23
166	Visualizing Virus Assembly Intermediates Inside Marine Cyanobacteria by Zernike Phase Contrast Electron Cryo-Tomography. Microscopy and Microanalysis, 2014, 20, 202-203.	0.2	1
167	Seeing the Portal in Membrane-containing Bacteriophage PRD1 by Cryo-EM. Microscopy and Microanalysis, 2014, 20, 1250-1251.	0.2	0
168	Identifying the assembly pathway of cyanophage inside the marine bacterium using electron cryo-tomography. Microbial Cell, 2014, 1, 45-47.	1.4	7
169	Cryo-EM Structure of a Molluscan Hemocyanin Suggests Its Allosteric Mechanism. Structure, 2013, 21, 604-613.	1.6	30
170	Visualizing virus assembly intermediates inside marine cyanobacteria. Nature, 2013, 502, 707-710.	13.7	123
171	Reprogramming an ATP-driven protein machine into a light-gated nanocage. Nature Nanotechnology, 2013, 8, 928-932.	15.6	55
172	Validation of Cryo-EM Structure of IP3R1 Channel. Structure, 2013, 21, 900-909.	1.6	43
173	Emdatabank: Unified Data Resource for 3DEM. Biophysical Journal, 2013, 104, 351a.	0.2	3
174	Cryo‣M model validation using independent map reconstructions. Protein Science, 2013, 22, 865-868.	3.1	72
175	Visualizing GroEL/ES in the Act of Encapsulating a Folding Protein. Cell, 2013, 153, 1354-1365.	13.5	102
176	Human CCT4 and CCT5 Chaperonin Subunits Expressed in Escherichia coli Form Biologically Active Homo-oligomers. Journal of Biological Chemistry, 2013, 288, 17734-17744.	1.6	54
177	Validated near-atomic resolution structure of bacteriophage epsilon15 derived from cryo-EM and modeling. Proceedings of the National Academy of Sciences of the United States of America, 2013, 110, 12301-12306.	3.3	68
178	EMEN2: An Object Oriented Database and Electronic Lab Notebook. Microscopy and Microanalysis, 2013, 19, 1-10.	0.2	52
179	TRiC's tricks inhibit huntingtin aggregation. ELife, 2013, 2, e00710.	2.8	73
180	Symmetry-free cryo-EM structures of the chaperonin TRiC along its ATPase-driven conformational cycle. EMBO Journal, 2012, 31, 720-730.	3.5	80

#	Article	IF	CITATIONS
181	A Tail-like Assembly at the Portal Vertex in Intact Herpes Simplex Type-1 Virions. PLoS Pathogens, 2012, 8, e1002961.	2.1	49
182	Paraneoplastic Thrombocytosis in Ovarian Cancer. New England Journal of Medicine, 2012, 366, 610-618.	13.9	651
183	Three-Dimensional Architecture of the Rod Sensory Cilium and Its Disruption in Retinal Neurodegeneration. Cell, 2012, 151, 1029-1041.	13.5	142
184	Filamentous, Mixed Micelles of Triblock Copolymers Enhance Tumor Localization of Indocyanine Green in a Murine Xenograft Model. Molecular Pharmaceutics, 2012, 9, 135-143.	2.3	46
185	An Examination of the Electrostatic Interactions between the N-Terminal Tail of the Brome Mosaic Virus Coat Protein and Encapsidated RNAs. Journal of Molecular Biology, 2012, 419, 284-300.	2.0	83
186	Supramolecular Non-Amyloid Intermediates in the Early Stages ofÂα-Synuclein Aggregation. Biophysical Journal, 2012, 102, 1127-1136.	0.2	31
187	Gorgon and pathwalking: Macromolecular modeling tools for subnanometer resolution density maps. Biopolymers, 2012, 97, 655-668.	1.2	45
188	Comparison of <i>Segger</i> and other methods for segmentation and rigidâ€body docking of molecular components in Cryoâ€EM density maps. Biopolymers, 2012, 97, 742-760.	1.2	68
189	The 2010 cryoâ€em modeling challenge. Biopolymers, 2012, 97, 651-654.	1.2	22
190	Constructing and Validating Initial Cα Models from Subnanometer Resolution Density Maps with Pathwalking. Structure, 2012, 20, 450-463.	1.6	38
191	The Molecular Architecture of the Eukaryotic Chaperonin TRiC/CCT. Structure, 2012, 20, 814-825.	1.6	261
192	Near-atomic resolution cryo-EM for molecular virology. Current Opinion in Virology, 2011, 1, 110-117.	2.6	46
193	Electron Cryo-Tomography of Cilia-Associated Structures of Rod Photoreceptors. Biophysical Journal, 2011, 100, 338a.	0.2	0
194	Dual Action of ATP Hydrolysis Couples Lid Closure to Substrate Release into the Group II Chaperonin Chamber. Cell, 2011, 144, 240-252.	13.5	94
195	Interbilayer-crosslinked multilamellar vesicles as synthetic vaccines for potent humoral and cellular immune responses. Nature Materials, 2011, 10, 243-251.	13.3	498
196	Cryo-EM Structure of a Group II Chaperonin in the Prehydrolysis ATP-Bound State Leading to Lid Closure. Structure, 2011, 19, 633-639.	1.6	52
197	Flexible Architecture of IP3R1 by Cryo-EM. Structure, 2011, 19, 1192-1199.	1.6	80
198	The group II chaperonin Mm pn binds and refolds human γD crystallin. Protein Science, 2011, 20, 30-41.	3.1	12

#	Article	IF	CITATIONS
199	Partially polymerized liposomes: stable against leakage yet capable of instantaneous release for remote controlled drug delivery. Nanotechnology, 2011, 22, 155605.	1.3	65
200	EMDataBank.org: unified data resource for CryoEM. Nucleic Acids Research, 2011, 39, D456-D464.	6.5	246
201	The Structure of Barmah Forest Virus as Revealed by Cryo-Electron Microscopy at a 6-Angstrom Resolution Has Detailed Transmembrane Protein Architecture and Interactions. Journal of Virology, 2011, 85, 9327-9333.	1.5	53
202	Structure of <i>Trypanosoma brucei</i> flagellum accounts for its bihelical motion. Proceedings of the National Academy of Sciences of the United States of America, 2011, 108, 11105-11108.	3.3	66
203	Structural basis for scaffolding-mediated assembly and maturation of a dsDNA virus. Proceedings of the United States of America, 2011, 108, 1355-1360.	3.3	191
204	4.4 Ã cryo-EM structure of an enveloped alphavirus Venezuelan equine encephalitis virus. EMBO Journal, 2011, 30, 3854-3863.	3.5	176
205	A Unique BSL-3 Cryo-Electron Microscopy Laboratory at UTMB. Applied Biosafety, 2010, 15, 130-136.	0.2	4
206	Zernike Phase Contrast Cryo-Electron Microscopy and Tomography for Structure Determination at Nanometer and Subnanometer Resolutions. Structure, 2010, 18, 903-912.	1.6	118
207	Structural changes in a marine podovirus associated with release of its genome into Prochlorococcus. Nature Structural and Molecular Biology, 2010, 17, 830-836.	3.6	136
208	Mechanism of folding chamber closure in a group II chaperonin. Nature, 2010, 463, 379-383.	13.7	196
209	Cryo-EM of macromolecular assemblies at near-atomic resolution. Nature Protocols, 2010, 5, 1697-1708.	5.5	79
210	4.0-â,,« resolution cryo-EM structure of the mammalian chaperonin TRiC/CCT reveals its unique subunit arrangement. Proceedings of the National Academy of Sciences of the United States of America, 2010, 107, 4967-4972.	3.3	152
211	Automated specimen search in cryo-TEM observation with DIFF-defocus imaging. Journal of Electron Microscopy, 2010, 59, 299-310.	0.9	12
212	Discrete Structure of an RNA Folding Intermediate Revealed by Cryo-electron Microscopy. Journal of the American Chemical Society, 2010, 132, 16352-16353.	6.6	29
213	Quantitative analysis of cryo-EM density map segmentation by watershed and scale-space filtering, and fitting of structures by alignment to regions. Journal of Structural Biology, 2010, 170, 427-438.	1.3	352
214	Visualizing the Structural Changes of Bacteriophage Epsilon15 and Its Salmonella Host during Infection. Journal of Molecular Biology, 2010, 402, 731-740.	2.0	59
215	Structure of a Conserved Retroviral RNA Packaging Element by NMR Spectroscopy and Cryo-Electron Tomography. Journal of Molecular Biology, 2010, 404, 751-772.	2.0	63
216	Model of human low-density lipoprotein and bound receptor based on CryoEM. Proceedings of the National Academy of Sciences of the United States of America, 2010, 107, 1059-1064.	3.3	65

#	Article	IF	CITATIONS
217	4.0 à Resolution Cryoâ€EM Structure of the Mammalian Chaperonin TRiC/CCT Reveals its Unique Subunit Arrangement. FASEB Journal, 2010, 24, 684.5.	0.2	0
218	Interprotofilament interactions between Alzheimer's Aβ _{1–42} peptides in amyloid fibrils revealed by cryoEM. Proceedings of the National Academy of Sciences of the United States of America, 2009, 106, 4653-4658.	3.3	147
219	Structural Mechanism of SDS-Induced Enzyme Activity of Scorpion Hemocyanin Revealed by Electron Cryomicroscopy. Structure, 2009, 17, 749-758.	1.6	61
220	Refinement of Protein Structures into Low-Resolution Density Maps Using Rosetta. Journal of Molecular Biology, 2009, 392, 181-190.	2.0	272
221	Effects of bilayer phases on phospholipid-poloxamer interactions. Soft Matter, 2009, 5, 1496.	1.2	36
222	Conformational Changes of Eukaryotic Chaperonin TRiC/CCT in the Nucleotide Cycle Revealed by CryoEM. FASEB Journal, 2009, 23, 850.12.	0.2	0
223	Rocking Motion of the Equatorial Domains of a Group II Chaperonin between Two Biochemical States Revealed by Singleâ€Particle Cryoâ€EM at Nearâ€atomic and Subnanometer Resolutions. FASEB Journal, 2009, 23, 673.12.	0.2	0
224	Backbone structure of the infectious ${\rm l}\mu15$ virus capsid revealed by electron cryomicroscopy. Nature, 2008, 451, 1130-1134.	13.7	204
225	Mechanism of lid closure in the eukaryotic chaperonin TRiC/CCT. Nature Structural and Molecular Biology, 2008, 15, 746-753.	3.6	91
226	Protein Structure Fitting and Refinement Guided by Cryo-EM Density. Structure, 2008, 16, 295-307.	1.6	334
227	De Novo Backbone Trace of GroEL from Single Particle Electron Cryomicroscopy. Structure, 2008, 16, 441-448.	1.6	164
228	Crystallographic Conformers of Actin in a Biologically Active Bundle of Filaments. Journal of Molecular Biology, 2008, 375, 331-336.	2.0	37
229	Location and Flexibility of the Unique C-Terminal Tail of Aquifex aeolicus Co-Chaperonin Protein 10 as Derived by Cryo-Electron Microscopy and Biophysical Techniques. Journal of Molecular Biology, 2008, 381, 707-717.	2.0	13
230	Remotely Triggered Liposome Release by Near-Infrared Light Absorption via Hollow Gold Nanoshells. Journal of the American Chemical Society, 2008, 130, 8175-8177.	6.6	471
231	Segmentation-free skeletonization of grayscale volumes for shape understanding. , 2008, , .		27
232	Subnanometer-resolution electron cryomicroscopy-based domain models for the cytoplasmic region of skeletal muscle RyR channel. Proceedings of the National Academy of Sciences of the United States of America, 2008, 105, 9610-9615.	3.3	106
233	Electron Cryotomography Reveals the Portal in the Herpesvirus Capsid. Journal of Virology, 2007, 81, 2065-2068.	1.5	81
234	Genome Sequence, Structural Proteins, and Capsid Organization of the Cyanophage Syn5: A "Horned― Bacteriophage of Marine Synechococcus. Journal of Molecular Biology, 2007, 368, 966-981.	2.0	92

#	Article	IF	CITATIONS
235	Singleâ€Particle Electron Cryomicroscopy of the Ion Channels in the Excitation–Contraction Coupling Junction. Methods in Cell Biology, 2007, 79, 407-435.	0.5	12
236	Learning-Based Segmentation Framework for Tissue Images Containing Gene Expression Data. IEEE Transactions on Medical Imaging, 2007, 26, 728-744.	5.4	19
237	Essential function of the built-in lid in the allosteric regulation of eukaryotic and archaeal chaperonins. Nature Structural and Molecular Biology, 2007, 14, 432-440.	3.6	96
238	Modular software platform for low-dose electron microscopy and tomography. Journal of Microscopy, 2007, 228, 384-389.	0.8	11
239	Identification of Secondary Structure Elements in Intermediate-Resolution Density Maps. Structure, 2007, 15, 7-19.	1.6	188
240	Refinement of Protein Structures by Iterative Comparative Modeling and CryoEM Density Fitting. Journal of Molecular Biology, 2006, 357, 1655-1668.	2.0	104
241	Structure of Halothiobacillus neapolitanus Carboxysomes by Cryo-electron Tomography. Journal of Molecular Biology, 2006, 364, 526-535.	2.0	139
242	Close membrane-membrane proximity induced by Ca2+-dependent multivalent binding of synaptotagmin-1 to phospholipids. Nature Structural and Molecular Biology, 2006, 13, 209-217.	3.6	235
243	Structure of epsilon15 bacteriophage reveals genome organization and DNA packaging/injection apparatus. Nature, 2006, 439, 612-616.	13.7	280
244	3D volume reconstruction of a mouse brain from histological sections using warp filtering. Journal of Neuroscience Methods, 2006, 156, 84-100.	1.3	83
245	Cryo-EM Asymmetric Reconstruction of Bacteriophage P22 Reveals Organization of its DNA Packaging and Infecting Machinery. Structure, 2006, 14, 1073-1082.	1.6	149
246	Outcome of a Workshop on Archiving Structural Models of Biological Macromolecules. Structure, 2006, 14, 1211-1217.	1.6	60
247	An Expanded Conformation of Single-Ring GroEL-GroES Complex Encapsulates an 86 kDa Substrate. Structure, 2006, 14, 1711-1722.	1.6	59
248	Structural biology of cellular machines. Trends in Cell Biology, 2006, 16, 144-150.	3.6	44
249	Ab Initio Modeling of the Herpesvirus VP26 Core Domain Assessed by CryoEM Density. PLoS Computational Biology, 2006, 2, e146.	1.5	54
250	Cryoelectron Microscopy of Protein IX-Modified Adenoviruses Suggests a New Position for the C Terminus of Protein IX. Journal of Virology, 2006, 80, 11881-11886.	1.5	33
251	Electron Cryomicroscopy of Biological Machines at Subnanometer Resolution. Structure, 2005, 13, 363-372.	1.6	138
252	Macromolecular Assemblies Highlighted. Structure, 2005, 13, 339-341.	1.6	5

#	Article	IF	CITATIONS
253	The Pore Structure of the Closed RyR1 Channel. Structure, 2005, 13, 1203-1211.	1.6	142
254	Building 3D surface networks from 2D curve networks with application to anatomical modeling. Visual Computer, 2005, 21, 764-773.	2.5	28
255	A Digital Atlas to Characterize the Mouse Brain Transcriptome. PLoS Computational Biology, 2005, 1, e41.	1.5	56
256	Common Ancestry of Herpesviruses and Tailed DNA Bacteriophages. Journal of Virology, 2005, 79, 14967-14970.	1.5	245
257	Structure of Ca2+ Release Channel at 14Ã Resolution. Journal of Molecular Biology, 2005, 345, 427-431.	2.0	76
258	Structural Analysis of the Anaphase-Promoting Complex Reveals Multiple Active Sites and Insights into Polyubiquitylation. Molecular Cell, 2005, 20, 855-866.	4.5	81
259	Superparamagnetic gadonanotubes are high-performance MRI contrast agents. Chemical Communications, 2005, , 3915.	2.2	310
260	The 3-Dimensional Architecture of Platelets in the Native State by Electron Cryotomography Blood, 2005, 106, 1658-1658.	0.6	1
261	A Digital Atlas to Characterize the Mouse Brain Transcriptome. PLoS Computational Biology, 2005, preprint, e41.	1.5	0
262	Mitochondrial ATP Synthasome. Journal of Biological Chemistry, 2004, 279, 31761-31768.	1.6	193
263	Structure of the bifunctional and Golgi-associated formiminotransferase cyclodeaminase octamer. EMBO Journal, 2004, 23, 2963-2971.	3.5	26
264	Structure of the acrosomal bundle. Nature, 2004, 431, 104-107.	13.7	75
265	Experimental Verification of Conformational Variation of Human Fatty Acid Synthase as Predicted by Normal Mode Analysis. Structure, 2004, 12, 185-191.	1.6	78
266	Seeing GroEL at 6 Ã Resolution by Single Particle Electron Cryomicroscopy. Structure, 2004, 12, 1129-1136.	1.6	187
267	Cryo-EM and Mass Spectrometry Based Investigations of Viral Capsid Morphogenesis. Microscopy and Microanalysis, 2004, 10, 226-227.	0.2	0
268	GroEL Structure at 6 Ã Resolution Using Electron Cryomicroscopy and EMAN. Microscopy and Microanalysis, 2004, 10, 1494-1495.	0.2	0
269	Subnanometer Imaging of Spherical Viruses in a JEOL3000 SFF Liquid Helium Electron Cryomicroscope. Microscopy and Microanalysis, 2004, 10, 1504-1505.	0.2	0
270	Structure of the herpesvirus major capsid protein. EMBO Journal, 2003, 22, 757-765.	3.5	88

#	Article	IF	CITATIONS
271	Coat protein fold and maturation transition of bacteriophage P22 seen at subnanometer resolutions. Nature Structural Biology, 2003, 10, 131-135.	9.7	190
272	Architecture of the Herpes Simplex Virus Major Capsid Protein Derived from Structural Bioinformatics. Journal of Molecular Biology, 2003, 331, 447-456.	2.0	30
273	The Structure of ClpB. Cell, 2003, 115, 229-240.	13.5	422
274	Structure of Isolated Nucleocapsids from Venezuelan Equine Encephalitis Virus and Implications for Assembly and Disassembly of Enveloped Virus. Journal of Virology, 2003, 77, 659-664.	1.5	29
275	Structure of the Type 1 Inositol 1,4,5-Trisphosphate Receptor Revealed by Electron Cryomicroscopy. Journal of Biological Chemistry, 2003, 278, 21319-21322.	1.6	85
276	Mitochondrial ATP Synthasome. Journal of Biological Chemistry, 2003, 278, 12305-12309.	1.6	171
277	Determination Of Icosahedral Virus structures By Electron Cryomicroscopy At Subnanometer Resolution. Advances in Protein Chemistry, 2003, 64, 93-124.	4.4	39
278	Studying Large Viruses. Advances in Protein Chemistry, 2003, 64, 379-408.	4.4	9
279	Imaging Ice Embedded Single Particles With A 16 Megapixel CCD Camera. Microscopy and Microanalysis, 2003, 9, 962-963.	0.2	0
280	High-Resolution 3D Reconstruction of Cytoplasmic Polyhedrosis Virus. Microscopy and Microanalysis, 2003, 9, 1366-1367.	0.2	0
281	Quaternary structure of human fatty acid synthase by electron cryomicroscopy. Proceedings of the National Academy of Sciences of the United States of America, 2002, 99, 138-143.	3.3	57
282	The skeletal muscle Ca2+ release channel has an oxidoreductase-like domain. Proceedings of the National Academy of Sciences of the United States of America, 2002, 99, 12155-12160.	3.3	60
283	Bilamellar Cationic Liposomes Protect Adenovectors from Preexisting Humoral Immune Responses. Molecular Therapy, 2002, 5, 233-241.	3.7	117
284	Electron cryo-microscopy of VAT, the archaeal p97/CDC48 homologue from Thermoplasma acidophilum 1 1Edited by D. Rees. Journal of Molecular Biology, 2002, 317, 673-681.	2.0	35
285	Merging Focal Pairs for Improved Particle Selection and Orientation Determination. Microscopy and Microanalysis, 2002, 8, 216-217.	0.2	0
286	Development of a Web Based Data Storage and Project Management System for Biological Electron Cryo-microscopy. Microscopy and Microanalysis, 2002, 8, 1576-1577.	0.2	0
287	Deriving folds of macromolecular complexes through electron cryomicroscopy and bioinformatics approaches. Current Opinion in Structural Biology, 2002, 12, 263-269.	2.6	47
288	Bridging the information gap: computational tools for intermediate resolution structure interpretation. Journal of Molecular Biology, 2001, 308, 1033-1044.	2.0	282

#	Article	IF	CITATIONS
289	Finding and using local symmetry in identifying lower domain movements in hexon subunits of the herpes simplex virus type 1 B capsid. Journal of Molecular Biology, 2001, 309, 903-914.	2.0	20
290	A 11.5 Ã single particle reconstruction of GroEL using EMAN. Journal of Molecular Biology, 2001, 314, 253-262.	2.0	119
291	Electron cryomicroscopy and bioinformatics suggest protein fold models for rice dwarf virus. Nature Structural Biology, 2001, 8, 868-873.	9.7	125
292	High resolution structural studies of complex icosahedral viruses: a brief overview. Virus Research, 2001, 82, 9-17.	1.1	17
293	Web-based Simulation for Contrast Transfer Function and Envelope Functions. Microscopy and Microanalysis, 2001, 7, 329-334.	0.2	2
294	Intrinsically disordered protein. Journal of Molecular Graphics and Modelling, 2001, 19, 26-59.	1.3	2,005
295	The Pattern of Tegument-Capsid Interaction in the Herpes Simplex Virus Type 1 Virion Is Not Influenced by the Small Hexon-Associated Protein VP26. Journal of Virology, 2001, 75, 11863-11867.	1.5	37
296	Venezuelan Equine Encephalomyelitis Virus Structure and Its Divergence from Old World Alphaviruses. Journal of Virology, 2001, 75, 9532-9537.	1.5	33
297	Web-based Simulation for Contrast Transfer Function and Envelope Functions. Microscopy and Microanalysis, 2001, 7, 329-334.	0.2	5
298	Web-based Simulation for Contrast Transfer Function and Envelope Functions. Microscopy and Microanalysis, 2001, 7, 329-334.	0.2	2
299	Electron Crystallographic Structure of the Limulus Acrosomal Bundle at 20 Ã Resolution. Microscopy and Microanalysis, 2000, 6, 242-243.	0.2	0
300	Macromolecular Structure Visualization Tools at NCMI. Microscopy and Microanalysis, 2000, 6, 282-283.	0.2	7
301	Estimates of the Fourier Amplitude Decay of Electron Micrographs of Single Particles. Microscopy and Microanalysis, 2000, 6, 256-257.	0.2	0
302	Identification of Additional Coat-Scaffolding Interactions in a Bacteriophage P22 Mutant Defective in Maturation. Journal of Virology, 2000, 74, 3871-3873.	1.5	23
303	Visualization of the maturation transition in bacteriophage P22 by electron cryomicroscopy. Journal of Molecular Biology, 2000, 297, 615-626.	2.0	68
304	Seeing the Herpesvirus Capsid at 8.5 Å . Science, 2000, 288, 877-880.	6.0	298
305	400 Kv Electron Cryo-Microscopic Imaging Of Large Icosahedral Viruses Towards Atomic Resolution. Microscopy and Microanalysis, 1999, 5, 186-187.	0.2	0
306	Solution X-Ray Scattering-Based Estimation of Electron Cryomicroscopy Imaging Parameters for Reconstruction of Virus Particles. Biophysical Journal, 1999, 76, 2249-2261.	0.2	34

#	Article	IF	CITATIONS
307	Mechanism of Scaffolding-Directed Virus Assembly Suggested by Comparison of Scaffolding-Containing and Scaffolding-Lacking P22 Procapsids. Biophysical Journal, 1999, 76, 3267-3277.	0.2	59
308	ADF/Cofilin weakens lateral contacts in the actin filament 1 1Edited by P. E. Wright. Journal of Molecular Biology, 1999, 291, 513-519.	2.0	86
309	The three-dimensional structure of the Limulus acrosomal process: a dynamic actin bundle 1 1Edited by W. Baumeister. Journal of Molecular Biology, 1999, 294, 139-149.	2.0	32
310	Visualization of Tegument-Capsid Interactions and DNA in Intact Herpes Simplex Virus Type 1 Virions. Journal of Virology, 1999, 73, 3210-3218.	1.5	229
311	Roles of Triplex and Scaffolding Proteins in Herpes Simplex Virus Type 1 Capsid Formation Suggested by Structures of Recombinant Particles. Journal of Virology, 1999, 73, 6821-6830.	1.5	49
312	Evaluation of charging on macromolecules in electron cryomicroscopy. Ultramicroscopy, 1998, 72, 41-52.	0.8	75
313	Multivariate analysis of single unit cells in electron crystallography. Ultramicroscopy, 1998, 74, 179-199.	0.8	23
314	Determination of the Gelsolin Binding Site on F-actin: Implications for Severing and Capping. Biophysical Journal, 1998, 74, 764-772.	0.2	64
315	Role of the Scaffolding Protein in P22 Procapsid Size Determination Suggested by T=4 and T=7 Procapsid Structures. Biophysical Journal, 1998, 74, 559-568.	0.2	90
316	Electron Crystallographic Analysis of Two-Dimensional Streptavidin Crystals Coordinated to Metal-Chelated Lipid Monolayers. Biophysical Journal, 1998, 74, 2674-2679.	0.2	19
317	Structure of Double-Shelled Rice Dwarf Virus. Journal of Virology, 1998, 72, 8541-8549.	1.5	59
318	Cofilin Changes the Twist of F-Actin: Implications for Actin Filament Dynamics and Cellular Function. Journal of Cell Biology, 1997, 138, 771-781.	2.3	685
319	An atomic model of the outer layer of the bluetongue virus core derived from X-ray crystallography and electron cryomicroscopy. Structure, 1997, 5, 885-893.	1.6	114
320	Electron crystallography of macromolecular periodic arrays on phospholipid monolayers. Advances in Biophysics, 1997, 34, 161-172.	0.6	30
321	Improved common line-based icosahedral particle image orientation estimation algorithms. Ultramicroscopy, 1997, 68, 231-255.	0.8	39
322	Three-dimensional Structure of Scaffolding-containing Phage P22 Procapsids by Electron Cryo-microscopy. Journal of Molecular Biology, 1996, 260, 85-98.	2.0	97
323	Two structural configurations of the skeletal muscle calcium release channel. Nature Structural and Molecular Biology, 1996, 3, 547-552.	3.6	161
324	Automatic Detection of Spherical Particles from Spot-Scan Electron Microscopy Images. Microscopy and Microanalysis, 1995, 1, 191-201.	0.2	7

Waн Chiu

#	Article	IF	CITATIONS
325	Electron cryomicroscopy and angular reconstitution used to visualize the skeletal muscle calcium release channel. Nature Structural Biology, 1995, 2, 18-24.	9.7	185
326	Assembly of VP26 in herpes simplex virus-1 inferred from structures of wild-type and recombinant capsids. Nature Structural and Molecular Biology, 1995, 2, 1026-1030.	3.6	152
327	Electron Cryomicroscopy of Bacillus stearothermophilus 50 S Ribosomal Subunits Crystallized on Phospholipid Monolayers. Journal of Molecular Biology, 1994, 239, 689-697.	2.0	35
328	Protein Subunit Structures in the Herpes Simplex Virus A-capsid Determined from 400 kV Spot-scan Electron Cryomicroscopy. Journal of Molecular Biology, 1994, 242, 456-469.	2.0	187
329	Low-dose thickness measurement of glucose-embedded protein crystals by electron energy loss spectroscopy and STEM dark-field imaging. Ultramicroscopy, 1993, 52, 157-166.	0.8	4
330	Flopping polypeptide chains and Suleika's subtle imperfections: analysis of variations in the electron micrograph of a purple membrane crystal. Ultramicroscopy, 1993, 49, 387-396.	0.8	15
331	Prospects for using an IVEM with a FEG for imaging macromolecules towards atomic resolution. Ultramicroscopy, 1993, 49, 407-416.	0.8	57
332	Electron crystallography of macromolecules. Current Opinion in Biotechnology, 1993, 4, 397-402.	3.3	5
333	Imaging Frozen, Hydrated Acrosomal Bundle from Limulus Sperm at 7 Ã Resolution with a 400 kV Electron Cryomicroscope. Journal of Molecular Biology, 1993, 230, 384-386.	2.0	18
334	Three-dimensional Transformation of Capsids Associated with Genome Packaging in a Bacterial Virus. Journal of Molecular Biology, 1993, 231, 65-74.	2.0	163
335	Computer-controlled spot-scan imaging of crotoxin complex crystals with 400 keV electrons at near-atomic resolution. Ultramicroscopy, 1992, 46, 229-240.	0.8	31
336	The thickness determination of organic crystals under low dose conditions using electron energy loss spectroscopy. Microscopy Research and Technique, 1992, 21, 166-170.	1.2	8
337	Analysis of symmetry and three-dimensional reconstruction of thin gp32â^—I crystals. Journal of Molecular Biology, 1991, 217, 551-562.	2.0	15
338	Three-dimensional structure of the HSV1 nucleocapsid. Cell, 1989, 56, 651-660.	13.5	164
339	Containment system for the preparation of vitrified-hydrated virus specimens. Journal of Electron Microscopy Technique, 1988, 8, 343-348.	1.1	22
340	The characterization of structural variations within a crystal field. Ultramicroscopy, 1988, 26, 345-360.	0.8	36
341	Atlas of plant viruses, volumes I and II. Micron and Microscopica Acta, 1988, 19, 115.	0.2	0
342	Cryo electron microscopy of unstained, unfixed RecA-cssDNA complexes. Journal of Structural Biology, 1988, 100, 166-172.	0.9	25

Waн Chiu

#	Article	IF	CITATIONS
343	Three-dimensional structural analysis of tetanus toxin by electron crystallography. Journal of Molecular Biology, 1988, 200, 367-375.	2.0	68
344	Three-dimensional structure of rotavirus. Journal of Molecular Biology, 1988, 199, 269-275.	2.0	363
345	High resolution cryo system designed for JEM 100CX electron microscope. Ultramicroscopy, 1987, 23, 61-66.	0.8	13
346	Potential for High-Resolution Electron Crystallography at Intermediate High Voltage. Annals of the New York Academy of Sciences, 1986, 483, 149-156.	1.8	7
347	Specimen preparative methods for electron crystallography of soluble proteins. Ultramicroscopy, 1984, 13, 19-25.	0.8	9
348	Experimental strategy in three-dimensional structure determination of crotoxin complex thin crystal. Ultramicroscopy, 1984, 13, 27-34.	0.8	6
349	Estimates of validity of projection approximation for three-dimensional reconstructions at high resolution. Ultramicroscopy, 1984, 14, 219-226.	0.8	40
350	Electron imaging of crotoxin complex thin crystal at 3.5 Ã Journal of Molecular Biology, 1984, 175, 93-97.	2.0	42
351	Quantitative assessment of radiation damage in a thin protein crystal. Journal of Microscopy, 1984, 136, 35-44.	0.8	37
352	Low dose electron microscopy of the crotoxin complex thin crystal. Journal of Molecular Biology, 1983, 164, 329-346.	2.0	45
353	Perspectives and outlook for electron microscopy in biology in general. Ultramicroscopy, 1982, 10, 165-177.	0.8	6
354	Effect of stray magnetic field on image resolution in transmission electron microscopy. Ultramicroscopy, 1980, 5, 351-356.	0.8	10
355	Structure of the surface layer protein of the outer membrane of Spirillum serpens. Journal of Ultrastructure Research, 1979, 66, 235-242.	1.4	39
356	Crystallization and preliminary electron diffraction study to 3.7 Ã of DNA helix-destabilizing protein gp32â^—I. Journal of Molecular Biology, 1978, 122, 103-107.	2.0	25
357	Single atom image contrast: conventional darkâ€field and brightâ€field electron microscopy. Journal of Microscopy, 1975, 103, 33-54.	0.8	17
358	A transform method for fast generalized image registration. , 0, , .		1